

Uncertainty Modeling and Analysis of the European XFEL Cavities Manufacturing Process

J. Corno,¹ N. Georg,^{1,2,*} S. Gorgi Zadeh,³ J. Heller,³ V. Gubarev,⁴ T. Roggen,⁵
U. Römer,² C. Schmidt,³ S. Schöps,¹ A. Sulimov,⁴ and U. van Rienen^{3,6}

¹*Technische Universität Darmstadt, Darmstadt, Germany*

²*Technische Universität Braunschweig, Braunschweig, Germany*

³*Universität Rostock, Rostock, Germany*

⁴*DESY, Hamburg, Germany*

⁵*CERN, Geneva, Switzerland*

⁶*Department Life, Light & Matter (LL&M), University of Rostock, Rostock, Germany*

This paper reports on comprehensive efforts on uncertainty quantification and global sensitivity analysis for accelerator cavity design. As a case study object the TESLA shaped superconducting cavities, as produced for the European X-ray Free Electron Laser (XFEL), are selected. The choice for these cavities is explained by the available measurement data that can be leveraged to substantiate the simulation model. Each step of the manufacturing chain is documented together with the involved uncertainties. Several of these steps are mimicked on the simulation side, e.g. by introducing a random eigenvalue problem. The uncertainties are then quantified numerically and in particular the sensitivities give valuable insight into the systems behavior. We also compare these findings to purely statistical studies carried out for the manufactured cavities. More advanced, adaptive, surrogate modeling techniques are adopted, which are crucial to incorporate a large number of uncertain parameters. The main contribution is the detailed comparison and fusion of measurement results for the XFEL cavities on the one hand and simulation based uncertainty studies on the other hand. After introducing the quantities of physical interest for accelerator cavities and the Maxwell eigenvalue problem, the details on the manufacturing of the XFEL cavities and measurements are reported. This is followed by uncertainty modeling with quantification studies.

I. INTRODUCTION

Accelerator devices require advanced, simulation based, design approaches due to demanding performance requirements and a considerable level of technical complexity. This is particularly true for superconducting accelerator cavities, which are a key element of many modern accelerator facilities. A typical design process involves 2D as well as 3D numerical solutions of the Maxwell eigenvalue problem, followed by optimization and uncertainty analysis and quantification studies. The latter have been conducted within the accelerator community from the 1970s, [1–3]. However, these studies have been mainly based on (local) sensitivity analysis which should be applied with care to quantify uncertainties in the cavities' geometry. Indeed, the eigenmodes and other measures of interest depend strongly on the shape of the cavity and local measures may not yield reliable results.

The topic of simulation based uncertainty quantification has seen tremendous developments in recent years, also in computational electromagnetics, see e.g. [4]. Nowadays, significant computational resources are available and uncertainty studies, taking into account systematically large parameter variations at all steps of the design process, come into reach. In particular, the concept of global sensitivity analysis [5] has received much attention, where sensitivities are characterized through the

contribution of each parameter (or parameter combination) to the variance of a system output quantity. Sobol sensitivity indices permit not only to analyze the importance of model input parameters, which in turn is useful in guiding modeling efforts, but also to identify important combined high-order parameter variations. Although the concept of global sensitivity analysis is well-established, the efficient computation of Sobol coefficients is a difficult task, mainly due to the complexity of the underlying eigenvalue problem [6]. This is addressed in the uncertainty literature by introducing surrogate models which emulate the relation between eigenmodes, or other quantities of interest on the model parameter.

In this respect, this paper reports on comprehensive efforts on uncertainty quantification and global sensitivity analysis for the simulation of TESLA shaped, superconducting, cavities. Such cavities have been produced in considerable quantity for the European X-ray Free Electron Laser (XFEL) and measurement data is available to substantiate the approach. Each step of the manufacturing chain is documented together with the involved uncertainties. Some of these steps are mimicked on the simulation side, e.g. by introducing a random eigenvalue problem. The uncertainties are then quantified numerically and in particular the sensitivities give valuable insight into the systems behavior. We also compare these findings to purely statistical studies carried out during the manufacturing. However, the simulation of all manufacturing steps would require the solution of several random inverse problems and is postponed to future work.

Uncertainty studies in an accelerator physics context

* n.georg@tu-braunschweig.de

have been reported before, see [7–9]. In this work, we use more advanced, adaptive, surrogate modeling techniques, which are crucial to incorporate a large number of uncertain parameters. The main contribution is the detailed comparison and fusion of real manufacturing data on the one hand and simulation based uncertainty studies on the other hand. The paper also clearly points out important directions of future research, which would allow to further combine measurements and simulation.

The structure of the paper is given as follows: Section II introduces quantities of physical interest for accelerator cavities and the Maxwell eigenvalue problem. In Section III, details on the manufacturing of the EXFEL cavities and measurements are reported. This is followed by uncertainty modeling and quantification studies in Section IV and concluding remarks.

II. CAVITIES AND MAXWELL EIGENVALUE PROBLEM

Accelerating cavities are devices used to accelerate particles to higher energies. Elliptical cavities are the accepted geometrical shape for particle velocities close to the speed of light ($\beta \approx 1$, where β is the ratio of particle velocity to the speed of light in vacuum). The shape of an elliptical cell is defined by two elliptical arcs connected by a tangent straight line as shown in FIG. 1. The fundamental mode of the cavity is the TM_{010} mode that is typically used as the operating mode of the cavity.

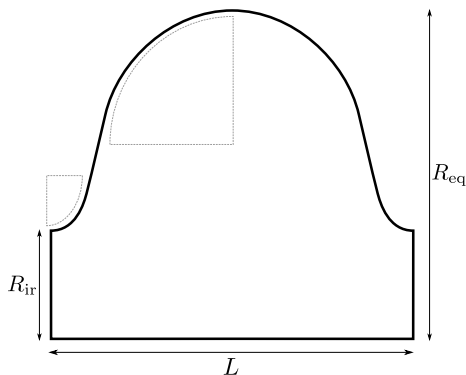


FIG. 1. Geometrical shape of an elliptical cell.

In order to enhance the accelerating efficiency, multi-cell cavities are created by connecting several cells together via their irises (see FIG. 2 for the EXFEL cavity described in more detail in Section III). Each mode of the single-cell generally divides into N_c modes of the same type in a multi-cell cavity with N_c cells and forms the so called passband of that mode. In this work, we are interested in the TESLA cavity shape [10], which is composed of $N_c = 9$ cells.

Let $\Omega(\mathbf{Y}) \subset \mathbb{R}^3$ refer to the inner domain of the multi-cell cavity with boundary $\partial\Omega(\mathbf{Y})$, where \mathbf{Y} denotes a vector of shape parameters to be specified. The fields in the

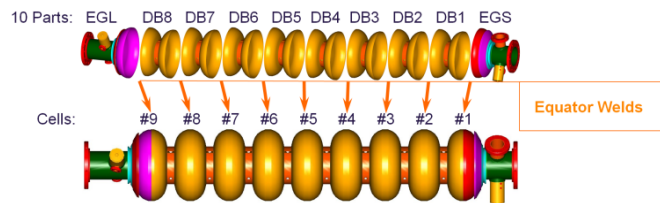


FIG. 2. The European XFEL cavity and its parts: 8 dumbbells (DB) and end-groups (EGS, EGL).

source-free, time-harmonic case, are given by Maxwell's equations:

$$\begin{aligned} \nabla \times \mathbf{E} &= -j\omega\mu_0\mathbf{H} & \nabla \times \mathbf{H} &= j\omega\epsilon_0\mathbf{E} \\ \nabla \cdot \epsilon_0\mathbf{E} &= 0 & \nabla \cdot \mu_0\mathbf{H} &= 0, \end{aligned} \quad (1)$$

where \mathbf{E} and \mathbf{H} denote the electric and magnetic field strength, ϵ_0 and μ_0 are the permittivity and permeability of vacuum, respectively. The walls are modeled as perfect electric conductor, i.e.,

$$\mathbf{E} \times \mathbf{n} = 0 \quad \mathbf{H} \cdot \mathbf{n} = 0. \quad (2)$$

One derives the Maxwell eigenvalue problem from (1) by eliminating \mathbf{H} . Introduction of the wave number $k = 2\pi f\sqrt{\mu_0\epsilon_0}$ yields

$$\begin{aligned} \nabla \times (\nabla \times \mathbf{E}) &= k^2\mathbf{E} \quad \text{in } \Omega(\mathbf{Y}) \\ \mathbf{E} \times \mathbf{n} &= 0 \quad \text{on } \partial\Omega(\mathbf{Y}), \end{aligned} \quad (3)$$

for $\mathbf{E} \neq 0$ and $\nabla \cdot \mathbf{E} = 0$. One should be aware that, although not explicitly specified, the field \mathbf{E} and the eigenfrequencies f depend on the shape parameters \mathbf{Y} . For each mode, i.e., a solution of (3) in the passband, there is a phase shift between fields of neighboring cells that can vary from 0 to π radians. The π -mode, with frequency f_π , of the TM_{010} passband is used in multi-cell cavities for acceleration.

In order to maximize the voltage across the cavity, the length of the middle-cells L is fixed as $L = \beta\lambda/2$, where λ refers to the wavelength of the π -mode, see [11]. Thus as the particle traverses a cell, the direction of the field reverses such that the particle is exposed to an identically directed electric field along the whole multi-cell cavity.

The modes in a passband have a small frequency difference. If the frequencies of the modes in the fundamental passband are very close to each other, there is a risk of exciting a mode close to f_π by the RF generator.

The spread of modes in the first passband is reflected in the cell-to-cell coupling coefficient, which is defined as [12]:

$$k_{cc} = 2 \frac{f_\pi - f_0}{f_\pi + f_0} \quad (4)$$

where f_0 refers to the lowest frequency in the passband. The cell-to-cell coupling coefficient is dimensionless and a sensitive quantity in the design phase. A large aperture

radius (R_{ir}) typically gives rise to a stronger cell-to-cell coupling.

If the energy of the fundamental mode is evenly distributed in the cells, the accelerating voltage is maximized [13, p.129]. Furthermore, a uniform field distribution allows for higher field magnitudes before reaching the surface electromagnetic (EM) field limit. The field flatness is a central figure of merit that indicates the uniformity of the field distribution of the fundamental mode between the cells. In this paper, the field flatness is defined as

$$\mathcal{F} = \frac{\min_{i=1,\dots,N_c} |E_{\text{ax,max}}^{(i)}|}{\max_{i=1,\dots,N_c} |E_{\text{ax,max}}^{(i)}|} \quad (5)$$

where $E_{\text{ax,max}}^{(i)}$ refers to the maximum axial electric field in cell i .

The resonant frequencies strongly depend on the geometry parameter in each cell, i.e., the equatorial radii $R_{\text{eq}}^{(i)}$, with $i = 1, \dots, N_c$, and the iris radii $R_{\text{ir}}^{(j)}$, with $j = 1, \dots, N_c + 1$. In Section IV we consider perturbations of the form $R_{\text{eq}}^{(i)} + \Delta R_{\text{eq}}^{(i)}$ and $R_{\text{ir}}^{(j)} + \Delta R_{\text{ir}}$ for the equatorial radii and the iris radius, respectively. Then, the parameter vector is given as

$$\mathbf{Y} = [\Delta R_{\text{eq}}^1, \dots, \Delta R_{\text{eq}}^9, \Delta R_{\text{ir}}]. \quad (6)$$

These perturbations change the resonant frequency of the respective cell(s) and consequently affect the frequency and the field distribution of the π -mode in the multi-cell cavity. It has been observed, that for the π -mode, the change in the field amplitude of each cell is proportional to the frequency change by a factor of N_c^2/k_{cc} [14, 15]. Thus, a small cell-to-cell coupling increases the sensitivity of the field profile with respect to geometrical perturbations.

III. CAVITY MANUFACTURING

The European X-ray Free Electron Laser [16] facility is constructed to produce X-ray pulses with the properties of laser light and at intensities much brighter than those produced by conventional synchrotron light sources. The superconducting linear accelerator of the EXFEL has a length of almost 2.1 km and brings electrons to an energy of up to 17.5 GeV. This is achieved by using a total of 808 superconducting cavities installed in the three main linac sections and the injector. The production of $N_{\text{cav}} > 808$ cavities [17], the largest in the history of cavity production, was realized by the two companies Research Instruments GmbH (RI) and Ettore Zanon S.p.A. (EZ). EXFEL uses nine-cell TESLA cavities build from solid niobium with a nominal $f_\pi = 1,300$ MHz. Each cavity (see FIG. 2) consists of 10 main sub-components, welded together at the equator area. The sub-components consist of 8 dumb-bells (DB) and 2 end-groups (EGL, EGS), referring to short and long end-groups, respectively. A

different shape of the end-groups' half-cells provides the desired asymmetry of the Higher Order Mode (HOM) field distributions and increases the efficiency of their extraction.

Geometric deviations of the inner cavity shape, the cavity length, and the spectra of frequencies as well as deviations in HOM field distributions occur due to random inaccuracies during manufacturing. These uncertainties have a strong impact on the quantities of interest described in Section II. Hence, dedicated measures are undertaken during production to ensure acceptable tolerances according to the EXFEL cavity specification, in particular to obtain $\mathcal{F} > 90\%$ and to keep the deviation of f_π below 100 kHz. These measures, together with sources of uncertainty, are summarized in FIG. 3 and described in detail in the following.

1. Step: Production

In this step $8N_{\text{cav}}$ DBs, consisting of 2 half cells each, N_{cav} EGSs and N_{cav} EGLs are produced.

2. Step: Trimming

The target of this step is to compensate for shape deviations by trimming the components. It is applied to all components (DB, EGS and EGL) and allows to obtain the necessary cavity length and frequencies with required accuracy.

3. Step: Selection and Sorting

The manufacturer selects two end groups and 8 dumb-bells. To minimize the influence of shape variations for the eight DBs on the asymmetry of the HOM field distribution, the DBs are sorted during the cavity assembly: a DB with average frequency is installed at the last position, the remaining DBs are installed in order of decreasing frequency (see FIG. 4).

4. Step: Welding

All components are welded, which induces shape deformations. The materials from the different suppliers exhibit different shrinkages at the welding joint. The resulting equator diameters may be slightly different depending on the cavity position during welding, see [19].

5. Step: Chemical treatment

The chemical treatment removes impurities and spikes, see [17], [20]. The homogeneity of the removed material from the cavity surface depends on many parameters of the process and the facility. The electrochemical polishing treatment is usually less homogeneous and more unstable than the equator welding.

6. Step: Tuning

The cavity is tuned, i.e., mechanically stretched or compressed, according to the procedure described by [21] which adjusts f_π with an accuracy of ± 50 kHz and ensures $\mathcal{F} > 98\%$ for the field flatness.

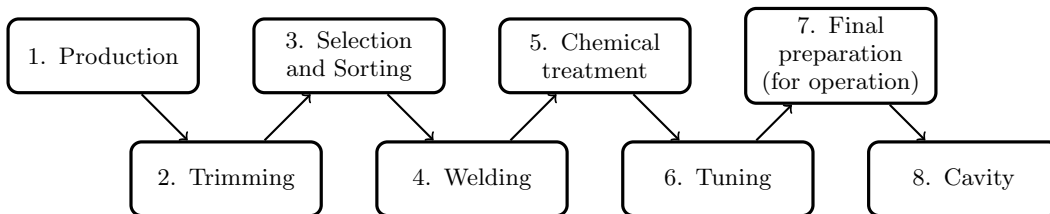


FIG. 3. Different steps of the TESLA cavity production chain.

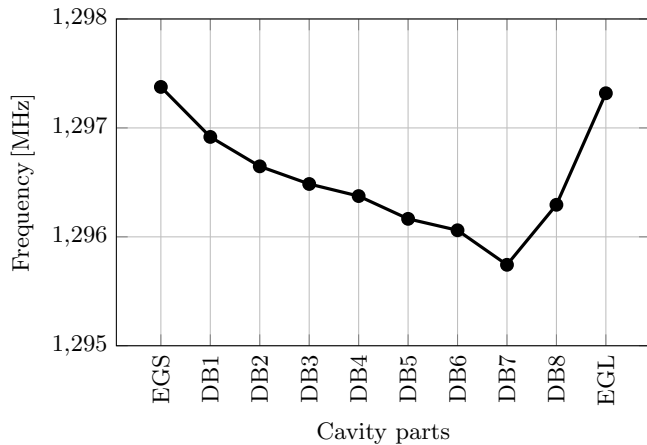


FIG. 4. Eigenfrequencies of dumb-bells and end-groups for an exemplary cavity from the DESY database [18].

7. Step: Final preparation (for operation)

The procedures applied in this step vary for different manufacturers and are shown in detail in FIG. 2 of [17]. Those procedures include, e.g., final buffered chemical polishing etching, the integration of the cavities into the Helium tanks, a pressure test using water under the pressure of 6 bar and the cool down to 2 K.

8. Step: Cavity

All N_{cav} cavities are operational and the statistics of the fundamental mode spectra are measured under 2 K. A description of the measurement procedures is given below.

Quality assurance by mechanical measurements of the inner surface dimensions becomes impossible after cavity welding and polishing. Measurement data can only be obtained by ultrasonic or RF measurements. These methods are used for control of equator welding stabilities [19] or homogeneity of the polishing process [20]. In the following the fundamental mode spectra are discussed for both manufactures based on RF measurements.

The measurements were carried out at operation temperature, i.e., cryogenic tests at 2 K were used (FIG. 5). The measurement results are presented in Table I. Note, that the π -mode finally operates at 1.3 GHz, which is ensured by an additional tuning step (not described here). The results show that the standard deviation of the

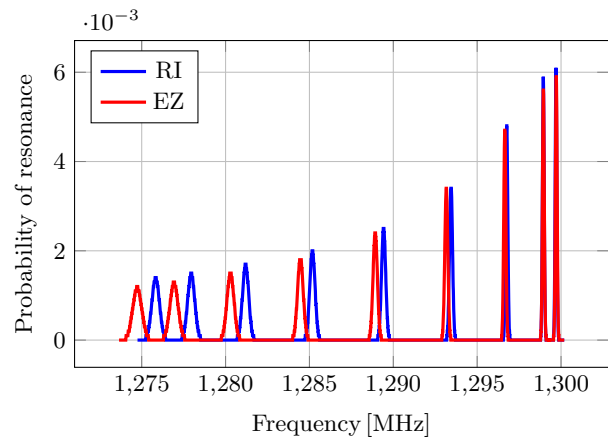


FIG. 5. Distribution of TM_{010} spectra for different manufacturers of the European XFEL cavities, data from [18].

π -mode (mode 8) in the relaxed condition after cool down, is about 50 kHz. This value increases with decreasing mode number. A similar behavior can be found for the differences

$$\Delta f_m = |\mathbb{E}[f_{\text{RI},m}] - \mathbb{E}[f_{\text{EZ},m}]|$$

of the averaged frequencies for each mode m between the two manufacturers RI and EZ, which also increases with decreasing mode number, see Tab. I. In particular, the difference of average frequencies is about 14 kHz for mode 8 and 1098 kHz for mode 0, respectively. These results indicate a high deviation of the cell-to-cell coupling coefficient between the manufacturers with

$$k_{\text{cc}} = (1.854 \pm 0.016) \% \text{ (RI) and} \\ k_{\text{cc}} = (1.941 \pm 0.021) \% \text{ (EZ),}$$

which are given in the form of average value plus/minus one standard deviation as obtained from database, see also Tab. IV. Preliminary studies [22] show that only variations of the iris radius can explain such high deviation in the cell-to-cell coupling coefficient. This will be analysed in more detail numerically in Section IV. Finally, the field flatness distribution for the EXFEL cavities is presented in FIG. 6. It can be observed that at least 70% of the cavities possess a field flatness of more than 95%.

TABLE I. TM₀₁₀ spectra for the European XFEL cavities, data taken from [18].

| Mode | Frequency, MHz | | | |
|------|----------------|----------|--------|-------|
| | Average | | St Dev | |
| | RI | EZ | RI | EZ |
| 0 | 1275.832 | 1274.734 | 0.226 | 0.268 |
| 1 | 1277.951 | 1276.926 | 0.212 | 0.245 |
| 2 | 1281.194 | 1280.294 | 0.186 | 0.208 |
| 3 | 1285.178 | 1284.460 | 0.157 | 0.168 |
| 4 | 1289.423 | 1288.921 | 0.124 | 0.129 |
| 5 | 1293.442 | 1293.161 | 0.089 | 0.090 |
| 6 | 1296.762 | 1296.649 | 0.064 | 0.066 |
| 7 | 1298.944 | 1298.946 | 0.052 | 0.054 |
| 8 | 1299.702 | 1299.716 | 0.050 | 0.052 |

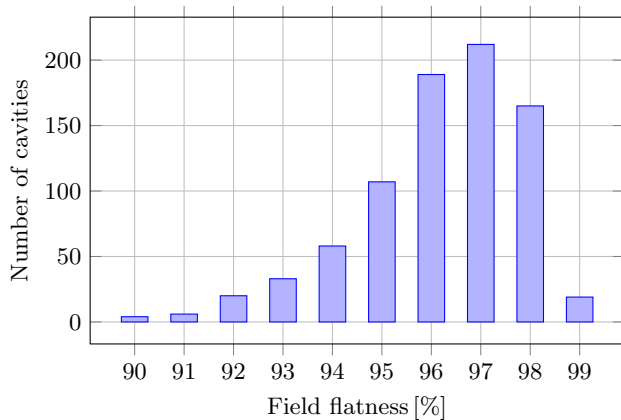


FIG. 6. Cavities with different field flatness, data taken from [18].

IV. UNCERTAINTY QUANTIFICATION

A stochastic setting is adopted here to model manufacturing and measurement uncertainties and assess their influence on the cavity design, i.e. each component of \mathbf{Y} becomes a random variable

$$\mathbf{Y}_{\text{prod}}(\theta) = [\Delta R_{\text{eq}}^1(\theta), \dots, \Delta R_{\text{eq}}^9(\theta), \Delta R_{\text{ir}}(\theta)] \quad (7)$$

where θ denotes a random outcome.

Uncertainty quantification encompasses various methods for uncertainty propagation, Bayesian inverse problems, optimal experimental design and robust optimization, among others. The reader is referred to [23–25] for a detailed background. In this work, uncertainty propagation is of great interest, in particular, propagating distributions of cell deformation parameters to distributions of quantities of interest, such as the cell-to-cell coupling coefficient. This can be achieved by sampling according to the underlying distribution and repetitively solving the cavity eigenvalue problem. Thereby, surrogate modeling is a key step to keep the computational workload manageable. The probability distributions of the cavity

geometry parameters are modeled based on descriptions of the manufacturing process, as described in Section III. A more general approach would consist in inferring these input distributions from measured RF data, which would require the solution of an inverse cavity eigenvalue problem. Such a study is out of the scope of the present work and can only be briefly addressed here, applying significant simplifications. In fact, the present study, should be considered as a step towards a more complete treatment of uncertainties in the cavity eigenvalue problem.

In this paper, calculations are carried out with the help of SUPERLANS code [26]. SUPERLANS is a 2D-axisymmetric finite-element-based code used for the calculation of the monopole modes of azimuthally symmetric geometries. For each simulation, the data describing the contour of the cavity is created by MATLAB [27] and saved in a format readable by SUPERLANS. SUPERLANS is then called by MATLAB to triangulate the geometry, solve the resulting eigenvalue problem and calculate the relevant secondary parameters. The results are finally read by MATLAB for the post-processing. The detailed description of the uncertainty modeling steps, which are the numerical counterpart of the production chain in Section III, are as following:

1. Step: Production

We generate $\tilde{N}_{\text{cav}} = 10^6$ random (“virtual”) cavities by creating, in turn, seven independent random mid cells and two end cells per cavity. In particular, those virtual cavities are obtained by drawing random numbers for the vector \mathbf{Y}_{prod} defined in (7) where we assume independence of the random variables. Although, the normal distribution seems to be the right choice, we opt for beta distribution in the range -0.3 mm to 0.3 mm. Beta distributions can be used to approximate normal distributions but have bounded support [24, Appendix B], which is very important in numerical studies to avoid non-physical parameter configurations. FIG. 7 represents such an approximation with probability density function (PDF)

$$\varrho(y) = \frac{140}{(u-l)^7} \begin{cases} (y-l)^3(u-y)^3, & l < y < u, \\ 0, & \text{else,} \end{cases}$$

where $l = -0.3$ mm and $u = 0.3$ mm denote the lower and upper bound, respectively. In this particular case the shape parameters of the beta distribution were chosen such that a normal distribution with a 2σ interval of -0.2 mm to 0.2 mm is approximated, as illustrated in FIG. 7.

2. Step: Trimming

In contrast to real manufacturing, in the simulation approach, we build cavities out of elementary cells instead of dumb-bells. In this setting, it is not clear how to explicitly model the trimming, however it is implicitly taken into account by the cavity length limitation (8) which is considered in the next step.

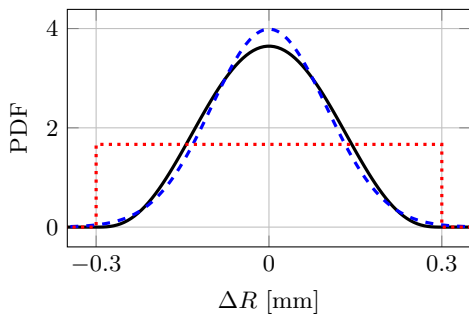


FIG. 7. Black: PDF of beta distributed radius variation with support in $[-0.3 \text{ mm}, 0.3 \text{ mm}]$. Blue, dashed: PDF of normal distribution with $\mu = 0 \text{ mm}$ and $\sigma = \frac{0.2}{2} \text{ mm}$. Red, dotted: PDF of uniform distribution with support in $[-0.3 \text{ mm}, 0.3 \text{ mm}]$.

3. Step: Selection and Sorting

The virtual 9-cell cavity is obtained from the random building blocks of step 1 as follows: We apply a sorting procedure which computes for all middle cells the fundamental resonance frequency (by solving a one-cell eigenvalue problem), places the cell closest to the average frequency at the 8th position and orders the remaining cells according to decreasing frequency between positions 2 and 7. Additionally, a total length constraint

$$\sum_{i=1}^{N_c} \Delta L^{(i)} < 3 \text{ mm} \quad (8)$$

is enforced. If the constraint is violated after tuning (step 6), the corresponding virtual cavity is disregarded. In real manufacturing, the constraint is already incorporated by trimming and compensation effects.

This selection and sorting influences the probability distribution. Hence, we introduce a new random vector $\mathbf{Y}_{\text{sort}}(\theta)$ where the density is estimated with kernel density techniques. In particular, we employ an Epanechnikov kernel [28] on the selected (and sorted) sample $\{\mathbf{Y}_{\text{sort}}^{(m)}\}_{m=1}^{\tilde{N}_{\text{sel}}}$ of size $\tilde{N}_{\text{sel}} = 691993$, which complies with the length constraint. The estimated densities are presented in Fig. 8.

4. Step: Welding

Again, since we consider cells instead of dumb-bells for the simulation, deformations during the welding procedure cannot be modeled properly and are therefore neglected.

5. Step: Chemical treatment

An appropriate modeling of chemical treatment would require very fine resolutions or even multi-scale analyses which is beyond the scope of the present paper.

6. Step: Tuning

The virtual tuning procedure we apply, considers

each cell individually and is therefore unable to incorporate field flatness constraints directly. However, we observe that an acceptable field flatness of at least 96% was obtained for all eigenvalue problems that are eventually solved. In particular, each cell is tuned to 1.3 GHz by changing its length $L^{(i)}$. Computationally, this requires the solution of a non-linear root finding problem for the objective function

$$f_{\text{obj}}^{(i)}(L^{(i)}) = f_0^{(i)}(L^{(i)}) - 1.3 \text{ GHz},$$

where $f_0^{(i)}$ denotes the fundamental eigenfrequency of cell i (one-cell eigenvalue problem). The root finding problem is solved using `fzero` in MATLAB.

In FIG. 9 the values of the 9-cell cavity accelerating frequency are depicted for different choices of the length and equatorial radius of the first cell. Considering the 1.3 GHz contour (in black in the figure), we observe that the tuning process correctly identifies a length such that a value of 1.3 GHz is obtained (the magenta dots in the figure lie on the contour line as expected).

7. Step: Final preparation (for operation)

Due to insufficient data and involved numerical modeling this step has to be neglected.

8. Step: Cavity

The Maxwell eigenvalue problem is solved to obtain the first nine modes for each virtual cavity and statistics of the spectra are computed. It shall be noted that, in general, eigenvalue tracking [6] should be employed to ensure a consistent matching of the eigenfrequencies. However, it has been observed that, in this case, the fundamental eigenfrequencies do not cross with respect to parameter changes for the considered variations. Hence, mode tracking is not applied here. The flow diagram of simulation steps is given in Fig. 10.

A. Stochastic Computations

In order to avoid the tremendous computational cost of repeatedly solving a large number of eigenvalue problems in step 3 and step 8, surrogate modeling is employed. In this work a dimension-adaptive Leja scheme [29] is used to construct accurate polynomial surrogate models. In particular, the algorithm described in [30, Chapter 3.2] is adapted to address the case of multiple quantities of interest. In order to obtain high uniform accuracies, we employ the classical unweighted Leja points. This algorithm constructs polynomial models adaptively which yields high computational efficiency. Moreover, we control the associated approximation errors by cross-validation to be sufficiently small.

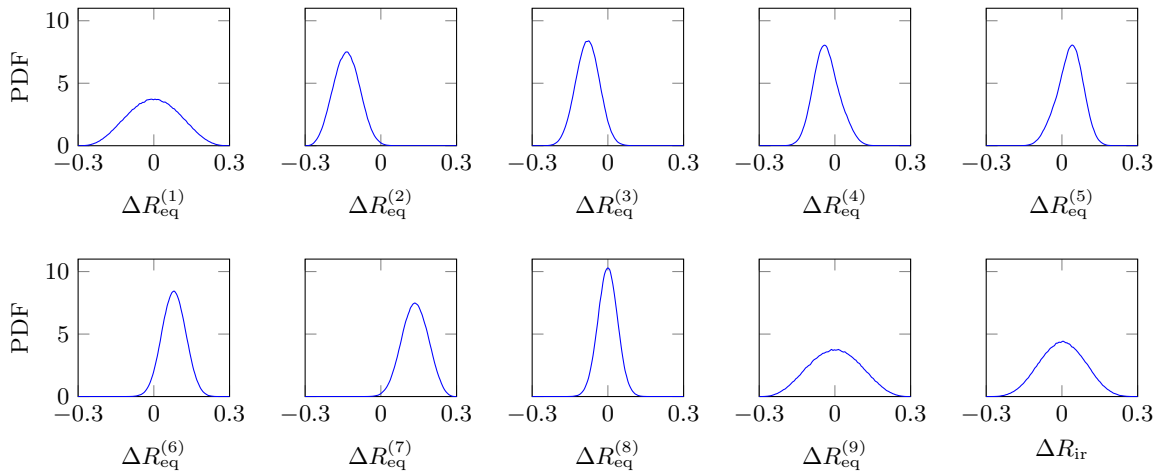


FIG. 8. Kernel density estimates of the 10 correlated input random variables.

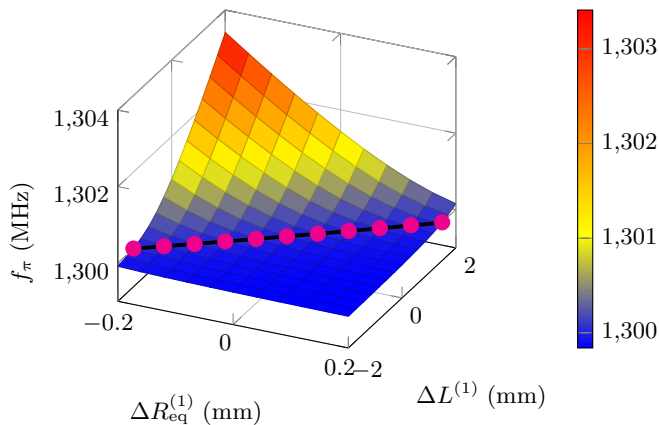


FIG. 9. The surface represents the accelerating frequency of the 9-cell cavity for different values of the changes in the equatorial radius $\Delta R_{\text{eq}}^{(1)}$ and in the length $\Delta L^{(1)}$ of cell 1. The black line is the 1.3 GHz contour line. The magenta points are the tuning values for $\Delta L^{(1)}$ obtained for a given value of $\Delta R_{\text{eq}}^{(1)}$.

The 3-variate polynomial surrogate models employed in step 3 are computed by solving 50 one-cell eigenvalue problems while 500 evaluations of the 9-cell eigenvalue problem are used to construct the 10-variate polynomial surrogate model for step 8. For all surrogate models, cross-validation with a uniformly distributed random sample of size 1000 indicates an error below 10 kHz for all fundamental resonance frequencies which is smaller than the standard expected deviations.

Now, all statistical quantities of interest can be obtained from the sample computed in step 8. In particular, we employ unbiased statistical estimates for the moments. The first two moments are depicted in FIG. 11 and Table II.

In the same way, we estimate the first four statistical moments of the cell-to-cell coupling coefficient k_{cc} ,

TABLE II. Mean values and standard deviations of the first passband in the tuned configuration.

| Mode | Mean [MHz] | Std. dev. [MHz] |
|------|------------|-----------------|
| 0 | 1,276.45 | 0.27 |
| 1 | 1,278.49 | 0.25 |
| 2 | 1,281.64 | 0.21 |
| 3 | 1,285.60 | 0.16 |
| 4 | 1,289.85 | 0.11 |
| 5 | 1,293.84 | 0.07 |
| 6 | 1,297.10 | 0.03 |
| 7 | 1,299.25 | 0.01 |
| 8 | 1,300.00 | 0.00 |

see Table III. To investigate the influence of the stochastic dependency in the input parameters, we additionally construct a sample of size \tilde{N}_{sel} containing independent realizations. This is achieved by sampling from the kernel-densities illustrated in FIG. 8. By, again, evaluating the surrogate model and using Monte Carlo estimates for this sample, the last column in Tab. III is obtained. Although, deviations can be observed, particularly in the even moments, the differences are small enough to resort to an independent analysis. Therefore, in the following, we employ Sobol indices as sensitivity measure, despite the fact that they are defined for independent parameters. Generalizations of Sobol indices for correlated data [31] exist but are not considered here. We use the OPEN-TURNS implementation of Saltelli's algorithm [32] to estimate Sobol indices of the cell-to-cell coupling coefficient for the 10 input parameters \mathbf{Y} . The results presented in FIG. 12 are obtained by evaluating $2(N+1) \cdot 10^6 = 22 \cdot 10^6$ times the surrogate model. As expected, the cell-to-cell coupling coefficient is heavily influenced by the iris radius while the equatorial radii have significantly less impact. In particular, more than 95% of the variation can be attributed to changes in the iris radius.

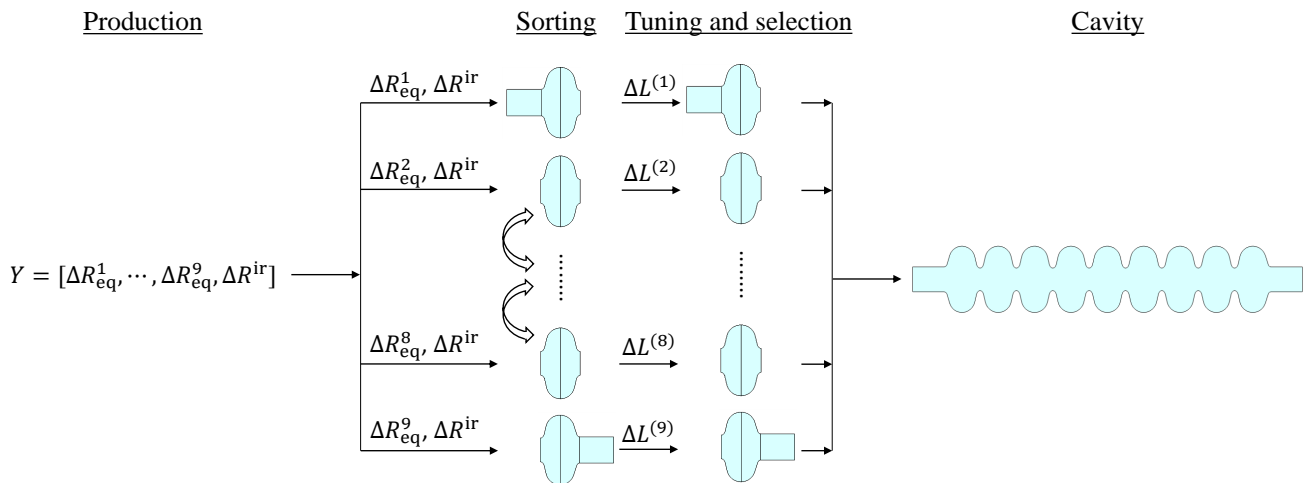
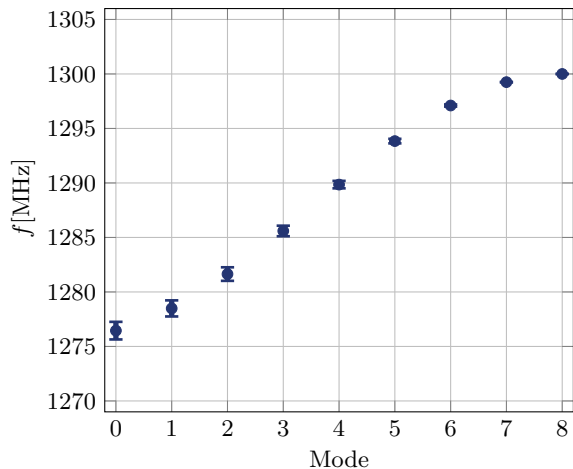
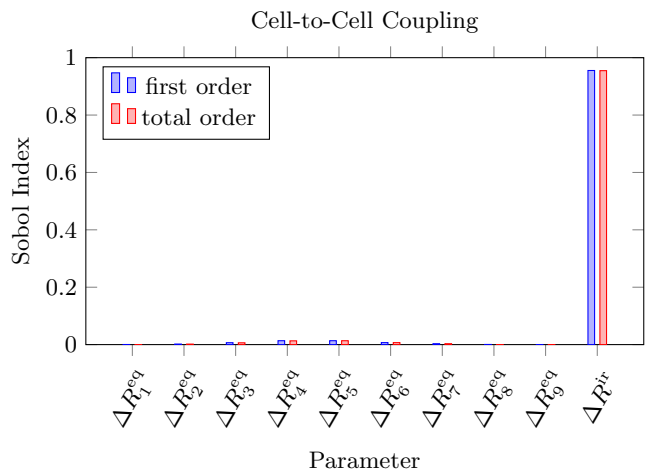


FIG. 10. The flow diagram of simulations steps.

FIG. 11. Mean values of the frequencies of the first passband with bars indicating the 3σ deviation intervals. Results are computed with the adaptive Leja sparse grid algorithm and 500 function evaluations.TABLE III. First four statistical moments of k_{cc} computed by either taking stochastic dependencies of parameters into account or modeling them as mutually independent.

| Moment | Stoch. dependent | Mut. independent |
|----------|------------------|------------------|
| Mean | 1.82807 | 1.82807 |
| Variance | 0.00045 | 0.00058 |
| Skewness | 0.01252 | 0.01336 |
| Kurtosis | -0.41521 | -0.33525 |

To conduct a preliminary inverse analysis, based on the previous findings, we neglect the deformations in the equatorial radii in the following. In this case, the task consists in estimating the parameter ΔR_{ir} from measurements of the cell-to-cell coupling coefficient k_{cc} . FIG. 13 depicts the associated relation which appears to be mono-

FIG. 12. Sobol indices for the cell-to-cell coupling k_{cc} .

tonic and almost linear in the considered range. We collected measurements of the fundamental mode spectra for $N_{cav} = 826$ cavities from the DESY Database [18]. Parameter estimation is then carried out by numerically inverting $\Delta R_{ir,i} \mapsto k_{cc,i}$, $i = 1, \dots, N_{cav}$. This is implemented by reformulating the root-finding problem as an optimization problem and applying the SCIPY implementation of the L-BFGS-B algorithm. Sample statistics are presented in Table IV.

The XFEL specification requires deviations in the iris radii before welding to be below 0.2mm with respect to the nominal value. It is expected that the mean values and deviations of the iris radii change during the production chain, for example the chemical treatment is considered to have a significant influence. This offset is estimated by our numerical model to be $\mathbb{E}[\Delta R_{ir,i}] = 0.243$ mm, cf. last row of Table IV. Despite this offset, the standard deviation $\text{Std}[R_{ir,i}]$ from both vendors are still within the limits of the speci-

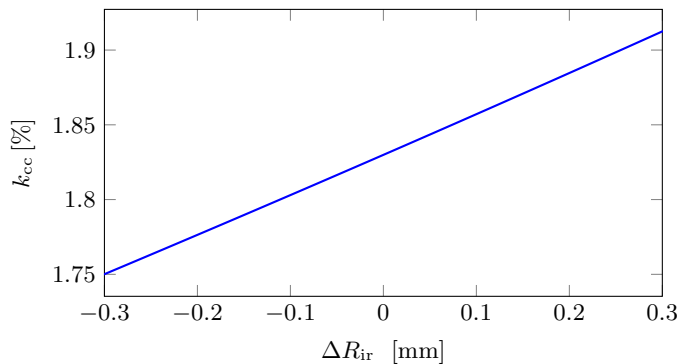


FIG. 13. Coupling coefficient k_{cc} with respect to change in iris radius R_{ir} .

TABLE IV. Empirical moments of cell-to-cell coupling coefficient for $N_{cav} = 826$ cavities as well as statistics about corresponding estimated iris deformations.

| Manufacturer | $\mathbb{E}[k_{cc,i}]$ | Std $[k_{cc,i}]$ | $\mathbb{E}[\Delta R_{ir,i}]$ | Std $[\Delta R_{ir,i}]$ |
|--------------|------------------------|------------------|-------------------------------|-------------------------|
| RI | 1.854 | 0.016 | 0.087 mm | 0.057 mm |
| EZ | 1.941 | 0.021 | 0.400 mm | 0.073 mm |
| RI+EZ | 1.897 | 0.047 | 0.243 mm | 0.170 mm |

fication ($0.17 \text{ mm} < 0.2 \text{ mm}$) after the full production chain. When considering the vendors separately, then both production processes, standard deviations 0.057 mm and 0.073 mm , operate approximately at a three-sigma level.

V. CONCLUSION

In this contribution the manufacturing chain of the EXFEL cavity was summarized and translated into a simulation workflow considering uncertainties. To analyze the sensitivities of the uncertain parameters, we propose an efficient adaptive surrogate modeling technique. The numerical study confirms the expert knowledge that the iris radius is the most critical parameter for the cell-to-cell coupling coefficient. Finally, the surrogate model is used to infer the first moments of the iris radius variations from frequency measurements. For both manufacturers the obtained standard deviations are within the specification.

The practically very relevant determination of stochastic moments for all design parameters from given measurements is still ongoing research, as well as the investigation of global sensitivities for HOM.

ACKNOWLEDGMENTS

The authors would like to acknowledge the support by the DFG (German Research Foundation) in the framework of the Scientific Network SCHM 3127/1,2 "Uncertainty quantification techniques and stochastic models for superconducting radio frequency cavities" that provided the basis for this collaborative work. The work of J. Corno, N. Georg and S. Schöps is supported by the Excellence Initiative of the German Federal and State Governments and the Graduate School of Computational Engineering at Technische Universität Darmstadt. N. Georg's work is also funded by the DFG grant RO4937/1-1. The work of S. Gorgi Zadeh was/is supported by the German Federal Ministry for Research and Education BMBF under contracts 05H15HRRBA and 05H18HRRB1, respectively. J. Heller's work was supported by the BMBF under the contracts 05K13HR1 and 05K16HRA.

-
- [1] K. Halbach and R. F. Holsinger. SUPERFISH – a computer program for evaluation of RF cavities with cylindrical symmetry. *Particle Accelerators*, 7:213–222, 1976.
 - [2] T. Weiland. A discretization model for the solution of Maxwell's equations for six-component fields. *Archiv Elektronik und Uebertragungstechnik*, 31:116–120, 1977.
 - [3] U. van Rienen and T. Weiland. Triangular discretization method for the evaluation of rf fields in waveguides and cylindrically symmetric cavities. *Particle Accelerators*, 20:239–265, 1987.
 - [4] S. Clénet. Uncertainty quantification in computational electromagnetics: The stochastic approach. *ICS Newsletter (International Compumag Society)*, 13:3–13, March 2013.
 - [5] I. M. Sobol'. On sensitivity estimation for nonlinear mathematical models. *Matematicheskoe Modelirovanie*, 2(1):112–118, 1990. *Mathematical Modeling & Computational Experiment (Engl.)*, 1993, 1, 407414.
 - [6] N. Georg, W. Ackermann, J. Corno, and S. Schöps. Uncertainty quantification for Maxwells eigenproblem using isogeometric analysis and mode tracking. *Comput. Meth. Appl. Mech. Eng.*, 350:228–244, March 2019.
 - [7] L. Xiao, C. Adolphsen, V. Akcelik, A. Kabel, K. Ko, L. Lee, Z. Li, and C. Ng. Modeling imperfection effects on dipole modes in TESLA cavity. In *IEEE Particle Accelerator Conference (PAC) 2007*, pages 2454–2456, June 2007.
 - [8] C. Schmidt, T. Flisgen, J. Heller, and U. van Rienen. Comparison of techniques for uncertainty quantification of superconducting radio frequency cavities. In Roberto D. Graglia, editor, *Proceedings of the International Conference on Electromagnetics in Advanced Applications (ICEAA) 2014*, pages 117–120. IEEE, August 2014.

- [9] J. Corno, C. de Falco, H. De Gerssem, and S. Schöps. Iso-geometric analysis simulation of TESLA cavities under uncertainty. In Roberto D. Graglia, editor, *Proceedings of the International Conference on Electromagnetics in Advanced Applications (ICEAA) 2015*, pages 1508–1511. IEEE, September 2015.
- [10] B. Aune, R. Bandelmann, D. Bloess, B. Bonin, A. Bosotti, M. Champion, et al. Superconducting TESLA cavities. *Physical Review Special Topics-Accelerators and Beams*, 3(9):092001, 2000.
- [11] H. Padamsee. Design topics for superconducting RF cavities and ancillaries. 2015.
- [12] S. Belomestnykh and V. Shemelin. High- β cavity design—a tutorial. In *The Proceedings of 12th International Workshop on RF Superconductivity (SRF2005)*, 2005.
- [13] H. Padamsee, J. Knobloch, and T. Hays. *RF Superconductivity for Accelerators*. John Wiley & sons., 1998.
- [14] J. Sekutowicz, M. Ferrario, and Ch. Tang. Superconducting superstructure for the TESLA collider: A concept. *Physical Review Special Topics-Accelerators and Beams*, 2(6):062001, 1999.
- [15] D. E. Nagle, E. A. Knapp, and B.C. Knapp. Coupled resonator model for standing wave accelerator tanks. *Rev. Sci. Instr.*, 38(11):1583–1587, 1967.
- [16] M. Altarelli, R. Brinkmann, M. Cherguiet, W. Decking, B. Dobson, S. Düsterer, et al. The Technical Design Report (TDR) of the European XFEL. DESY 2006-097, July 2007.
- [17] W. Singer, A. Brinkmann, R. Brinkmann, J. Iversen, A. Matheisen, W. D. Moeller, A. Navitski, D. Reschke, J. Schaffran, A. Sulimov, et al. Production of superconducting 1.3-GHz cavities for the European X-ray Free Electron Laser. *Phys. Rev. Accel. Beams*, 19:092001, 2016.
- [18] A. Sulimov and H. Weise. DESY cavity database. http://xfel.desy.de/cavity_database/. accessed: 2019-05-16.
- [19] A. Sulimov. RF analysis of equator welding stability for the european XFEL cavities. In *Proceedings of The 17th International Conference on RF Superconductivity, SRF 2015, Whistler, BC, Canada*, 2015.
- [20] A. Sulimov, A. Visentin, M. Giarretta, and A. Gresele. RF analysis of electropolishing for EXFEL cavities production at Ettore Zanon Spa. In *Proceedings of The 28th Linear Accelerator Conference, LINAC16, East Lansing, MI, USA*, 2017.
- [21] G. R. Kreps, J. Sekutowicz, and D. Proch. Tuning of the TESLA superconducting cavities and the measurement of higher order mode damping. In *Proceedings of the XVth Conference on Charged Particle Accelerators, Dubna, Russia*, 1996.
- [22] A. Sulimov, G. Kreps, J. Sekutowicz, et al. Estimation of small geometry deviation for tesla-shape cavities due to inner surface polishing. In *Proceedings of The 16th International Conference on RF Superconductivity, SRF 2013, Paris, France*, page 537, 2013.
- [23] R. G. Ghanem and P. D. Spanos. Stochastic finite element method: Response statistics. In *Stochastic finite elements: a spectral approach*, pages 101–119. Springer, 1991.
- [24] D. Xiu. *Numerical Methods for Stochastic Computations: A Spectral Method Approach*. Princeton University Press, 2010.
- [25] O. Le Maître and O. M. Knio. *Spectral methods for uncertainty quantification: with applications to computational fluid dynamics*. Springer Science & Business Media, 2010.
- [26] D. G. Myakishev and V. P. Yakovlev. An interactive code SUPERLANS for evaluation of RF-cavities and acceleration structures. In *Conference Record of the 1991 IEEE Particle Accelerator Conference*, pages 3002–3004 vol.5, May 1991.
- [27] MATLAB. *Version R2017b*. The MathWorks, Inc., Natick, Massachusetts, USA, 2017.
- [28] V. A. Epanechnikov. Non-parametric estimation of a multivariate probability density. *Theory Probab. Appl.*, 14(1):153–158, 1969.
- [29] A. Narayan and J. D. Jakeman. Adaptive Leja sparse grid constructions for stochastic collocation and high-dimensional approximation. *SIAM J. Sci. Comput.*, 36(6):A2952–A2983, 2014.
- [30] N. Georg, D. Loukrezis, U. Römer, and S. Schöps. Uncertainty quantification for an optical grating coupler with an adjoint-based Leja adaptive collocation method. *arXiv preprint arXiv:1807.07485*, 2018.
- [31] C. Xu and G. Gertner. Extending a global sensitivity analysis technique to models with correlated parameters. *Comput. Statist. Data Anal.*, 51(12):5579–5590, 2007.
- [32] A. Saltelli. Making best use of model evaluations to compute sensitivity indices. *Comput. Phys. Commun.*, 145(2):280–297, 2002.